Heliyon 10 (2024) e34704

Contents lists available at ScienceDirect

Heliyon

journal homepage: www.cell.com/heliyon

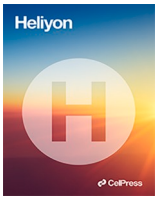

Research article

Gene signature developed based on programmed cell death to predict the therapeutic response and prognosis for liver hepatocellular carcinoma

Lijun Tian [a], Yujie Sang [a], Bing Han [a], Yujing Sun [a], Xueyan Li [b], Yuemin Feng [b], Chengyong Qin [a,b,**], Jianni Qi [c,d,*]

[a] Department of Gastroenterology, Shandong Provincial Hospital, Shandong University, Jinan, 250021, China
[b] Department of Gastroenterology, Shandong Provincial Hospital Affiliated to Shandong First Medical University, Jinan, 250021, China
[c] Central Laboratory, Shandong Provincial Hospital, Shandong University, Jinan, 250021, China
[d] Central Laboratory, Shandong Provincial Hospital Affiliated to Shandong First Medical University, Jinan, 250021, China

ARTICLE INFO

Keywords:
Drug sensitivity
Programmed cell death
Preoperative prediction model
Prognosis
Liver hepatocellular carcinoma

ABSTRACT

Background: The prognosis and therapeutic response of patients with liver hepatocellular carcinoma (LIHC) can be predicted based on programmed cell death (PCD) as PCD plays a crucial role during tumor progression. We developed a PCD-related gene signature to evaluate the therapeutic response and prognosis for patients with LIHC.

Methods: Molecular subtypes of LIHC were classified using ConsensusClusterPlus according to the gene biomarkers related to PCD. To predict the prognosis of high- and low-risk LIHC patients, a risk model was established by LASSO regression analysis based on the prognostic genes. Functional enrichment analysis was conducted using clusterProfiler package, and relative abundance of immune cells was quantified applying CIBERSORT package. Finally, to determine drug sensitivity, oncoPredict package was employed.

Results: PCD was correlated with the clinicopathologic features of LIHC. Then, we defined four molecular subtypes (C1–C4) of LIHC using PCD-related prognostic genes. Specifically, subtype C1 had the worst prognosis with enriched T cells regulatory (Tregs) and Macrophage_M0 and higher expression of T cell exhaustion markers, meanwhile, C1 also had a relatively higher TIDE score and metastasis potential. A risk model was established using 5 prognostic genes. High-risk patients tended to have higher expression of T cell exhaustion markers and TIDE score and unfavorable outcomes, and they were more sensitive to small molecule drug 5.Fluorouracil.

Conclusion: A PCD-related gene signature was developed and verified to be able to accurately predict the prognosis and drug sensitivity of LIHC patients.

1. Introduction

Liver cancer (LC) is a frequently detected cancer that ranks the third highest cause of cancer-correlated mortality worldwide [1]. Liver hepatocellular carcinoma (LIHC) comprises 75–85 % of primary LC and is the most prevalent subtype of LC that shows a poor

* Corresponding author. Central Laboratory, Shandong Provincial Hospital, Shandong University, Jinan, 250021, China.
** Corresponding author. Department of Gastroenterology, Shandong Provincial Hospital, Shandong University, Jinan, 250021, China.
E-mail addresses: chengyong_qin@126.com (C. Qin), slqijn@126.com (J. Qi).

https://doi.org/10.1016/j.heliyon.2024.e34704
Received 13 February 2024; Received in revised form 15 May 2024; Accepted 15 July 2024

prognosis and high recurrence [2,3]. Recent development in both systemic and locoregional therapies have contributed greatly to LIHC management [4]. However, these novel therapeutic strategies still fail to achieve universal applicability, and LIHC patients may exhibit therapeutic resistance to these therapies [5]. Evidence demonstrates that only a limited proportion of patients could benefit from taking some systemic treatments [6]. Therefore, developing novel prognosis prediction methods and precision treatment for LIHC has become an urgent task in clinical practice [7].

Cancers are a result of failure in immunological control and resistance of transformed cells against cell death signaling pathways [8]. Cell death governs outcomes and long-term sequelae in almost all hepatic disease conditions [9]. PCD is also a type of regulated cell death but it is an autonomous process regulated by genes for cells to maintain homeostatic balance [10]. The initiation and regulation of diverse PCD types involve broad crosstalk, which has emerged as research focus in oncological studies [11]. Together with lately discovered cuproptosis and disulfidptosis, PCD mainly includes alkaliptosis and oxeiptosis, necroptosis, apoptosis, autophagy, pyroptosis, entosis, NETosis, ferroptosis, lysosome-dependent cell death, and parthanatos, which all play critical roles in both homeostasis and diseases such as cancers [12,13]. To study the relationship between PCD and LIHC, bioinformatics analysis and experimental validation have identified PCD index for improving the prognostic evaluation and therapy response for LIHC patients [10]. A novel cuproptosis-related gene signature has also been developed to predict the prognosis of LIHC [14]. A cuproptosis-related risk score could be used to evaluate the prognosis and characterize the tumor microenvironment in LIHC [15]. Another pyroptosis-related gene signature also shows a high accuracy in estimating the prognosis and immune activity in LIHC [16]. Furthermore, previous study screened non-apoptotic PCD-related differentially expressed genes (DEGs) to predict the prognosis, cancer stemness, tumor microenvironment (TME) and Transarterial Chemoembolization (TACE) response for LIHC patients [15].

Considering the role of PCD-correlated genes in evaluating the prognosis and drug sensitivity, our current study defined the molecular subtypes of LIHC and developed a PCD-related prognostic signature, the robustness of which was verified in both ICGC-LIRI-JP and GSE76427 datasets. To conclude, our study classified molecular subtypes and mined PCD-related genes for the prognostic evaluation and selection of relevant therapeutic targets for LIHC patients.

2. Methods

2.1. Data collection and pre-processing

1) The RNA-seq data of primary LIHC samples (n = 371) from the TCGA database were obtained via TCGA GDC API and pre-processed as follows: samples without clinical follow-up status or data were eliminated. Gene symbol IDs were transformed based on the Ensembl gene IDs, and when a gene had multiple Gene symbol IDs, the average value was taken to indicate the gene expression.
2) The ICGC-LIRI-JP dataset containing 212 LIHC samples was obtained from the Hepatocellular Carcinoma Database (HCCDB) (http://lifeome.net/database/hccdb/).
3) GSE76427 containing the gene expression profile of LIHC was downloaded from the GEO dataset. After sorting, only 115 samples were retained. The probes were mapped to genes based on the annotation information, and average value was taken to indicate gene expression when multiple probes matched one gene.

TCGA-LIHC was a training set, with ICGC-LIRI-JP and GSE76427 as the independent validation sets in this study.

2.2. Molecular subtyping based on genes correlated with PCD

PCD-related genes came from a previous study [17]. The “Pam” algorithm and “Euclidean distance” served as the metric distance. Using “ConsensusClusterPlus” package, samples in the TCGA-LIHC dataset were subjected to 500 bootstraps with each bootstrap running 80 % of the samples to test result stability [18]. Cumulative distribution function (CDF) was analyzed to help define the optimal number (k = 4) of clusters. The number of clusters typically relies on a smooth growth of the CDF climbing up to an inflection point, after which a slower growth could indicate that adding more clusters will no longer significantly improve the clustering consistency. Finally, the progression-free survival and overall survival of each subtype of LIHC were evaluated, and the corresponding results were shown in the Kaplan-Meier (KM) curves with the log-rank test.

2.3. Establishment of a prognostic model and verification

Under false discovery rate (FDR) < 0.05 and $|\log_2 FC| > \log_2(1.5)$, the DEGs were selected based on the molecular subtypes using limma package [19]. Subsequently, the DEGs conforming to $|\log_2 FC| > \log_2(1.5)$ and P-value <0.05 were selected and subjected to univariate Cox regression analysis (P-value <0.05). LASSO analysis was performed using the "glmnet" R package together with 5-fold cross validation to determine the optimal λ value. To identify the genes that contributed most to the model, Stepwise Akaike information criterion (stepAIC) was conducted using the MASS package [20,21].

The prognostic signature developed using the PCD-related genes for LIHC patients was as follow [22]:

$$\text{Risk score} = \sum \beta i * \text{ExPi}$$

(β: the coefficient value calculated via Cox regression analysis; i: gene expression level)

Each sample in the training set TCGA-LIHC was assigned with a risk score, followed by the zscore standardization. Accordingly,

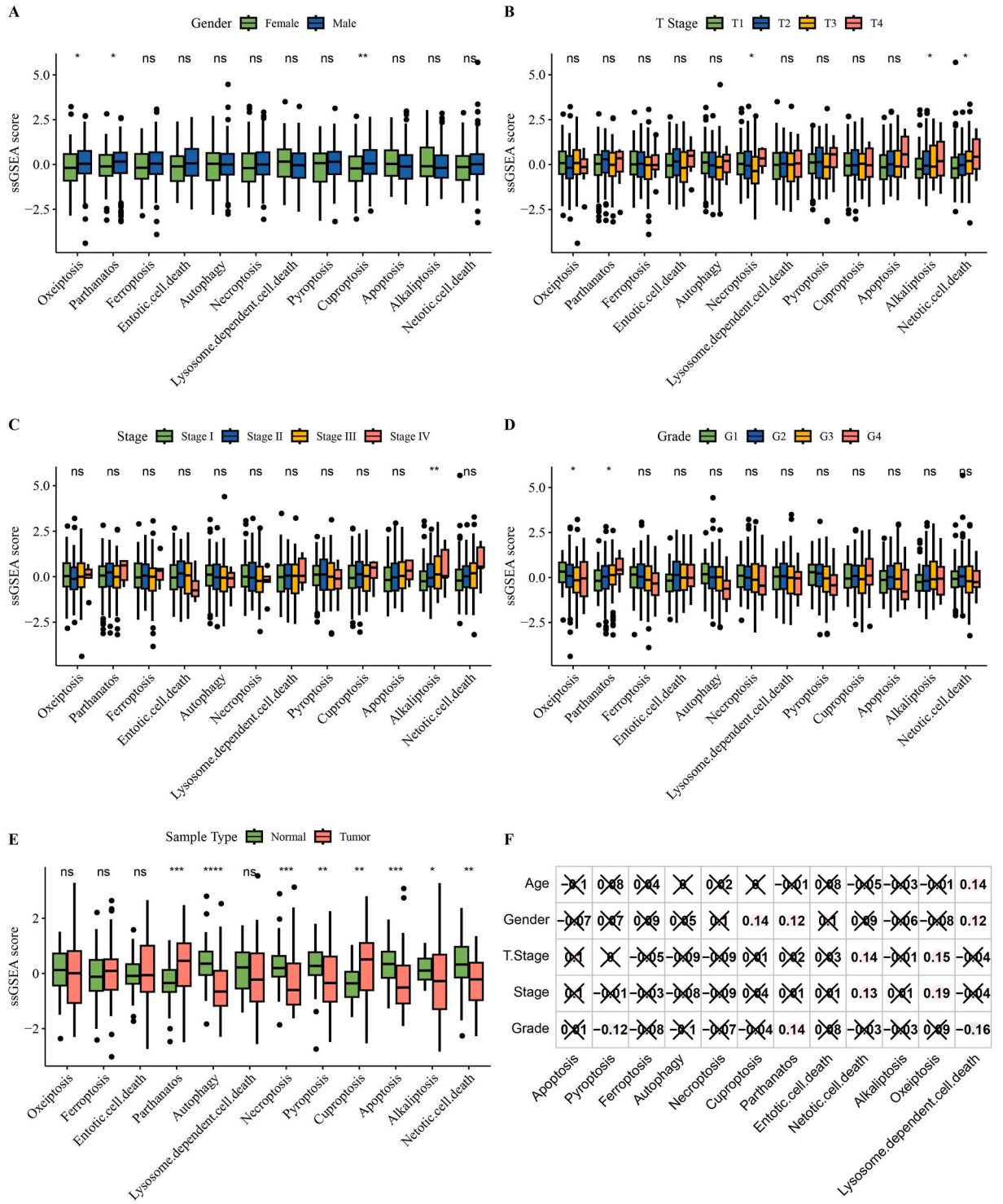

Fig. 1. The association between the PCD and the clinicopathologic features of patients in TCGA-LIHC. A-D, Differential enrichment score of PCD in the clinicopathological features of patients in TCGA-LIHC, including gender, T stage, Stage and Grade. E, Differences on the PCD in normal and tumor tissue in TCGA-LIHC. F, Correlation in PCD and the clinicopathologic features of patients in TCGA-LIHC. ns represents$P > 0.05$. *$P < 0.05$; **$P < 0.01$; ***$P < 0.001$; ****$P < 0.0001$.

high- and low-risk groups of samples were classified under the threshold of 0 and subjected to prognosis analysis using KM curve. The receiver operating characteristic (ROC) curve was drawn using "timeROC" package to test the model robustness in the ICGC-LIRI-JP and GSE76427 [23,24].

2.4. Determination on the characteristics of relevant pathways

Differential pathways with FDR <0.05 in each subtype were analyzed by performing gene set enrichment analysis (GSEA) on Kyoto Encyclopedia of Genes and Genomes (KEGG) pathways. Functional enrichment analysis was conducted using "ClusterProfiler" package [25].

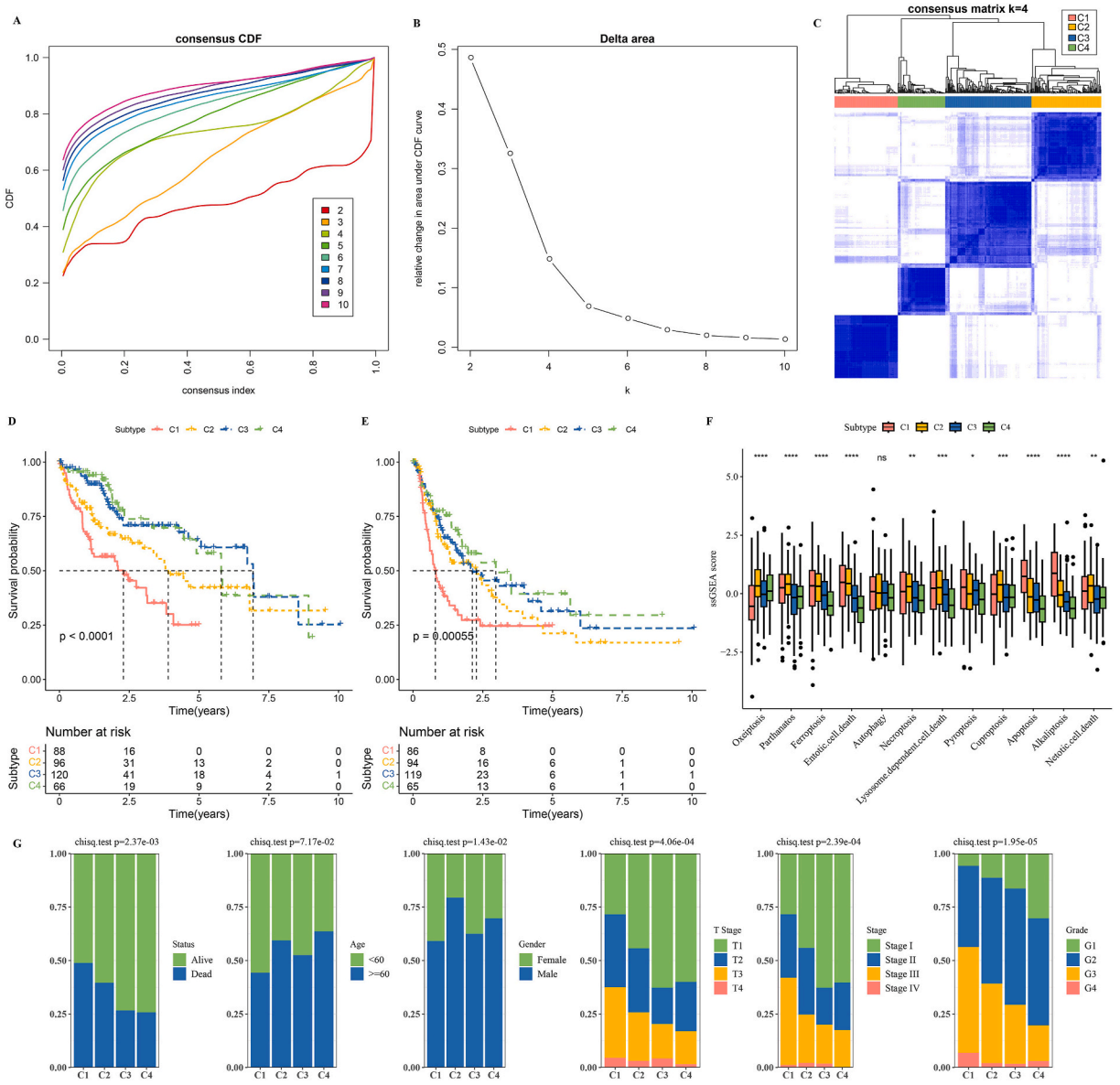

Fig. 2. Identification on the molecular subtypes based on PCD-related genes. A, Consensus cumulative distribution function plot. B, Delta area plot showing the relative change in area under the CDF curve C, Consensus matrix heat map displaying consensus values on a white to blue color scale for each cluster of patients. D, Kaplan-Meier curve of the 4 molecular subtypes in TCGA-LIHC. E, Progression-free survival time of the 4 molecular subtypes in TCGA-LIHC; F, Difference on the PCD in 4 molecular subtypes in TCGA-LIHC. G, Difference on the clinicopathologic features in molecular subtypes in TCGA-LIHC. ns represents$P > 0.05$. *$P < 0.05$; **$P < 0.01$; ***$P < 0.001$; ****$P < 0.0001$.

2.5. Immune microenvironment analysis

To comprehensively investigate the relationship between immune microenvironment in LIHC and the risk score, the relative abundance of 22 types of immune cells in LIHC samples was calculated using CIBERSORT algorithm (https://cibersort.stanford.edu/) [26]. MCP-counter, TIMER, and EPIC were also employed to determine the immune cell infiltration in different subtypes or risk groups.

2.6. Sensitivity test of the risk model

The sensitivity of LIHC patients in different risk groups to anti-tumor drugs was determined using the estimated IC_{50} value with the "oncoPredict" package [27]. Further analysis was conducted to explore the association between the risk score and estimated IC_{50} value. The results with an adjusted FDR <0.05 (by Benjamini-Hochberg method) were defined as having a significantly close relationship with the drugs.

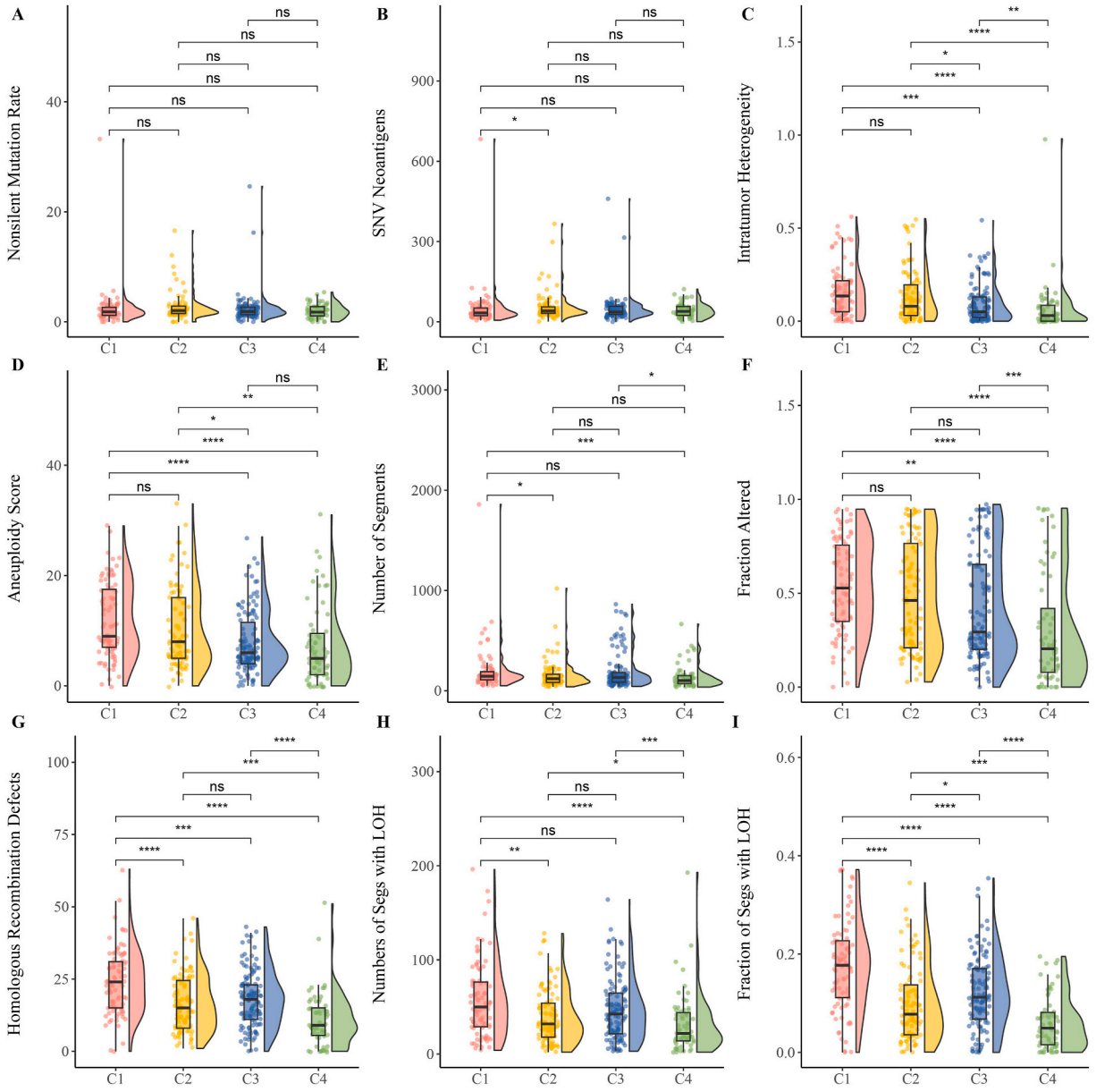

Fig. 3. Determination on the genomic landscape alternations among the molecular subtypes. A-I, The genomic landscape alternations among the molecular subtypes (C1, C2, C3 and C4) in TCGA-LIHC cohort. ns represents$P > 0.05$. *$P < 0.05$; **$P < 0.01$; ***$P < 0.001$; ****$P < 0.0001$.

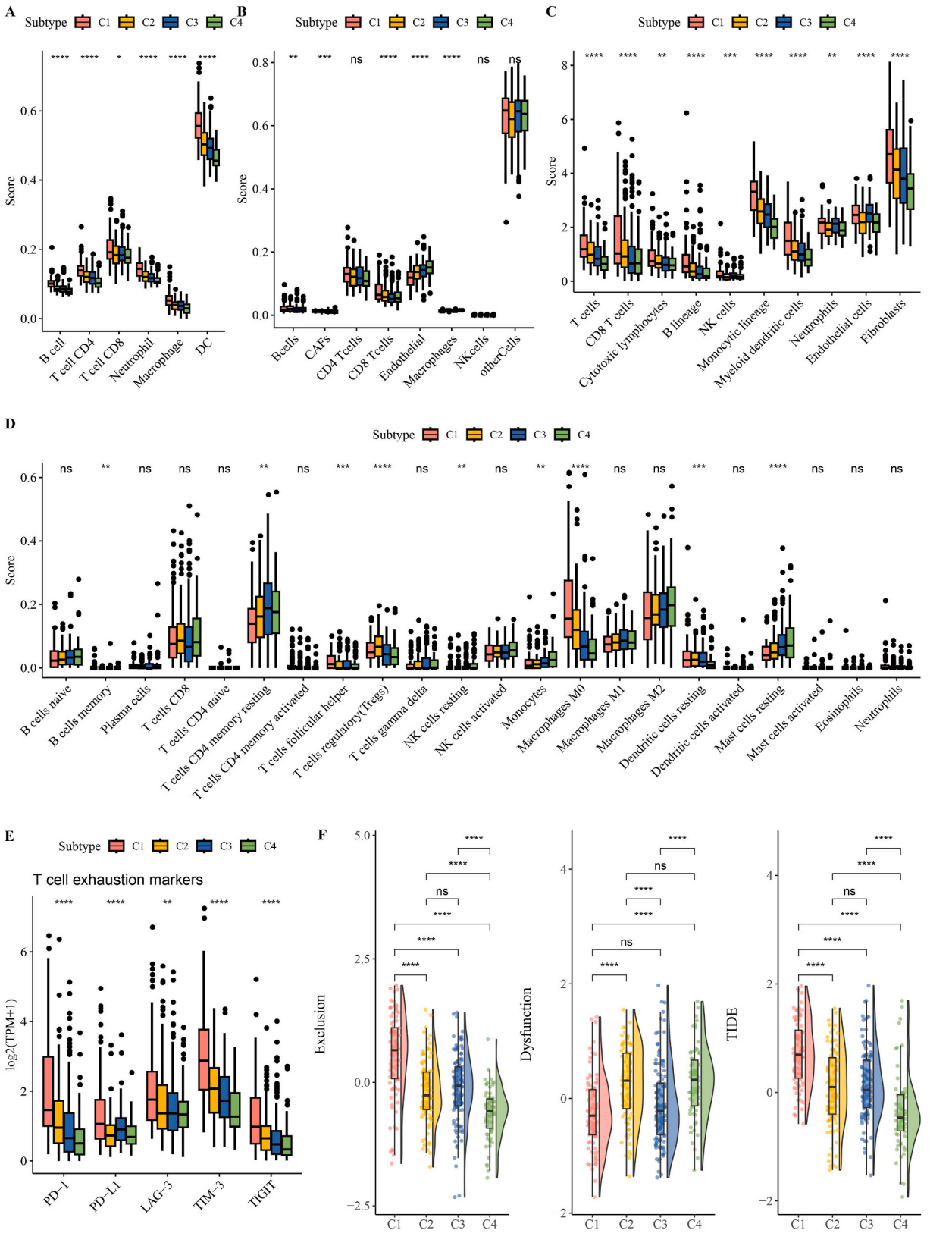

(caption on next page)

Fig. 4. Analysis on the immune microenvironment among 4 molecular subtypes.
A-D, Immune cells score in different molecular subtypes (C1, C2, C3 and C4) of TCGA-LIHC cohort, as determined via TIMER, EPIC, MCP-counter and CIBERSORT. E, Expression levels of T cell exhaustion markers in different molecular subtypes (C1, C2, C3 and C4) of TCGA-LIHC cohort. F, Differences on the predicted T cell dysfunction scores, T cell exclusion scores and TIDE score in different molecular subtypes (C1, C2, C3 and C4) of TCGA-LIHC cohort. ns represents$P > 0.05$. *$P < 0.05$; **$P < 0.01$; ***$P < 0.001$; ****$P < 0.0001$.

2.7. Statistical analyses

R package (version 3.6.3) was used in all data analyses. FDR was adjusted using Benjamin and Hochberg method. Significant differences in the survival analysis were defined by log-rank test, and the KM method was utilized in survival analysis. Wilcox rank-sum test and Kruskal-Wallis test were used for comparing differences in PCD scores between LIHC and para-cancer tissues and for assessing differences between different clinical characteristics, respectively. The chi-square test was used to detect the somatic mutation among subtypes and compare the distribution of clinicopathologic features in different subtypes or risk groups. Applying Spearman correlation analysis, correlation study was performed. Statistically significant was defined when $P < 0.05$.

3. Results

3.1. The association between the clinicopathologic features of patients in TCGA-LIHC and PCD

The enrichment score of the signature genes related to 12 types of PCD in TCGA cohort was computed via ssGSEA. Here, T stage, Stage, Grade and Gender showed significant differences in PCD. In detail, male and low-grade patients had higher score of oxeiptosis and parthanotos, while the scores of alkaliptosis and netotic cell death were relatively higher in T stage and Stage (Fig. 1A–D). Meanwhile, most PCD was significantly enriched in LIHC patients (Fig. 1E). Correlation analysis showed that lysosome-dependent cell death and age and alkaloptosis and netotic cell death were significantly correlated with T stage and stage (Fig. 1F).

3.2. Defining molecular subtypes using PCD-related genes

A total of 335 PCD-correlated genes were identified to be significantly related to the prognosis ($P < 0.01$). Consensus clustering analysis results demonstrated a relatively stable CDF curve when the number of clusters was 4 (Fig. 2A and B), thus, 4 molecular subtypes (C1, C2, C3 and C4) were defined (Fig. 2C). The results from survival analysis (shown in KM curve) unveiled the most favorable prognosis in subtype C4 and the worst prognosis in subtype C1 (Fig. 2D and E). Also, we compared the differences in the PCD score of these subtypes and observed significant difference in the PCD score in these subtypes (Fig. 2F). Fig. 2G displayed the distribution of different clinicopathologic features in different molecular subtypes, it can be seen that subtype C1 had more advanced stage and higher grade (see Fig. 3).

3.3. The genomic landscape alternations of the 4 molecular subtypes

The molecular features of the 4 subtypes in TCGA-LIHC collected from a previous study [28]. According to the results, greater intratumor heterogeneity, higher numbers of Segs with LOH and fraction of Segs with LOH, number of segments, fraction altered, aneuploidy score, homologous recombination defects were seen in subtype C1 (Fig. 3A–I).

3.4. The immune microenvironment among the 4 molecular subtypes

Gene expression in the immune cells was used to evaluate the degree of immune cells infiltration in TCGA-LIHC cohort so as to further compare the differences of the immune microenvironment in the 4 molecular subtypes TIMER, EPIC, and MCP-counter were also applied at the same time. As shown in Fig. 4A–C, subtype C1 had different types of enriched immune cells and stromal cells. Moreover, the results of CIBERSORT (Fig. 4D) showed that Treg and Macrophages_M0 were evidently enriched in subtype C1.

Comparison on the expressions of T cell exhaustion markers in these 4 molecular subtypes demonstrated that the levels of TIGIT, LAG-3, TIM-3, PD-L1, and PD-1 were relatively higher in subtype C1, followed by subtype C3, while those in subtype C4 were relatively lower (Fig. 4E).

Differences in patients' response to immunotherapy were also analyzed. As depicted in Fig. 4F, subtype C1 had a higher TIDE score, indicating limited immunotherapy benefit for C1 patients. Moreover, comparison on predicted T cell dysfunction scores and T cell exclusion scores among the molecular subtypes showed that subtype C1 had the highest T cell exclusion score. These results showed that gene expression in the C1 subtype was related to a worse prognosis and high immune evasion, which may serve as a new biomarker to improve the personalized therapeutic treatment for LIHC patients.

3.5. The characteristics of relevant pathways among 4 molecular subtypes

Under the thresholds of FDR <0.05 and $|\log2FC| > \log2$, "limma" package was employed to calculate the DEGs among these 4 molecular subtypes (C1 vs other, C2 vs other, C3 vs other, and C4 vs other) at (1.5). Specifically, 7272 DEGs were identified in subtype

C1 (528 downregulated and 6744 upregulated genes), 745 DEGs were identified in subtype C2 (580 downregulated and 165 upregulated genes), 574 DEGs were identified in subtype C3 (176 downregulated and 398 upregulated genes) and 5192 DEGs were identified in subtype C4 (4948 downregulated and 244 upregulated genes) (Fig. 5A). Then these DEGs were intersected in a Venn diagram, resulting in a total of 52 genes as the common DEGs among these subtypes (Fig. 5B).

"ClusterProfiler" was then applied for the functional enrichment analysis on these common DEGs in these molecular subtypes, and the relevant results were seen in Fig. 5C. In C1 subtype, the upregulated genes were greatly enriched in cell cycle-related pathways, while those of C4 subtype were enriched in metabolism-related pathways. Meanwhile, the enriched pathways of downregulated genes among these molecular subtypes were also compared (Fig. 5D). Further comparison on the differences in metastasis-related pathways (NF-kappa B signaling pathway, JAK/STAT signaling pathway, TGF-beta signaling pathway, Notch signaling pathway, Wnt signaling pathway, and VEGF signaling pathway) showed higher ssGSEA scores in C1 subtype (Fig. 5E).

3.6. *Establishment of a prognostic signature and validation*

A total of 33 genes (24 "Risk" and 9 "Protective" genes) closely related to the prognosis were identified from the aforementioned 52 common genes using univariate Cox regression analysis ($P < 0.05$). The number of genes in the risk model was reduced using LASSO. Fig. 6A displayed the trajectory of each independent variable with lambda. Increased lambda was positively related to increased number of independent variable coefficients approaching 0. To examine the confidence interval under each lambda, 3-fold cross-validation was applied (Fig. 6B). We screened 11 genes as genes of interest when lambda = 0.0524, and finally 5 genes were

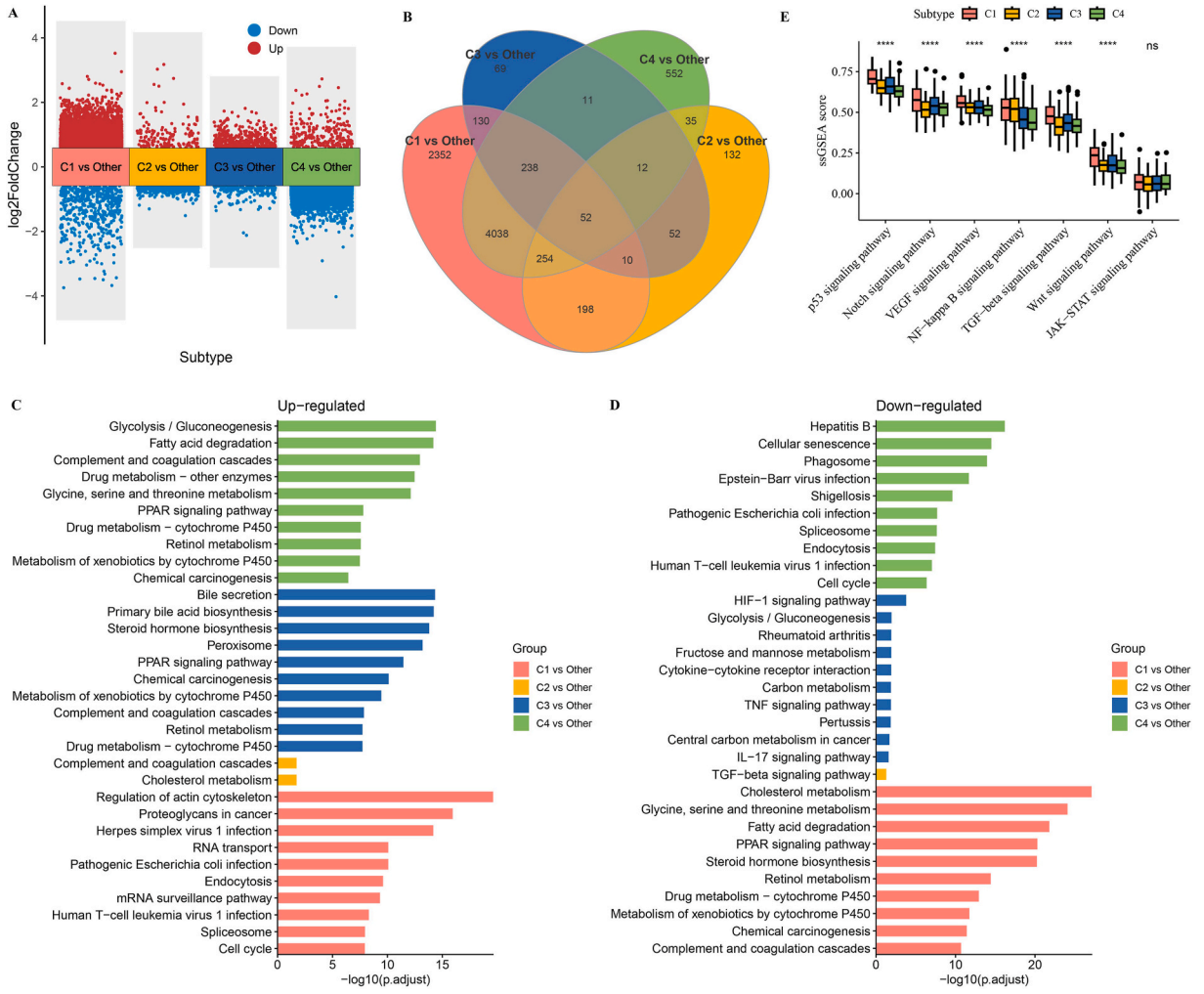

Fig. 5. Characteristics of relevant pathways among 4 molecular subtypes
A, DEGs of the 4 molecular subtypes (C1, C2, C3 and C4) in TCGA-LIHC cohort, as depicted in a Volcano plot. B, Common DEGs across the four molecular subtypes (C1, C2, C3 and C4) in TCGA-LIHC cohort intersected via a Venn diagram. C, D, Enriched pathways of upregulated and downregulated genes in the four molecular subtypes (C1, C2, C3 and C4) in TCGA-LIHC cohort (top 10). E, ssGSEA score of metastasis-related pathways in the four molecular subtypes (C1, C2, C3 and C4) in TCGA-LIHC cohort. ns represents$P > 0.05$; ****$P < 0.0001$.

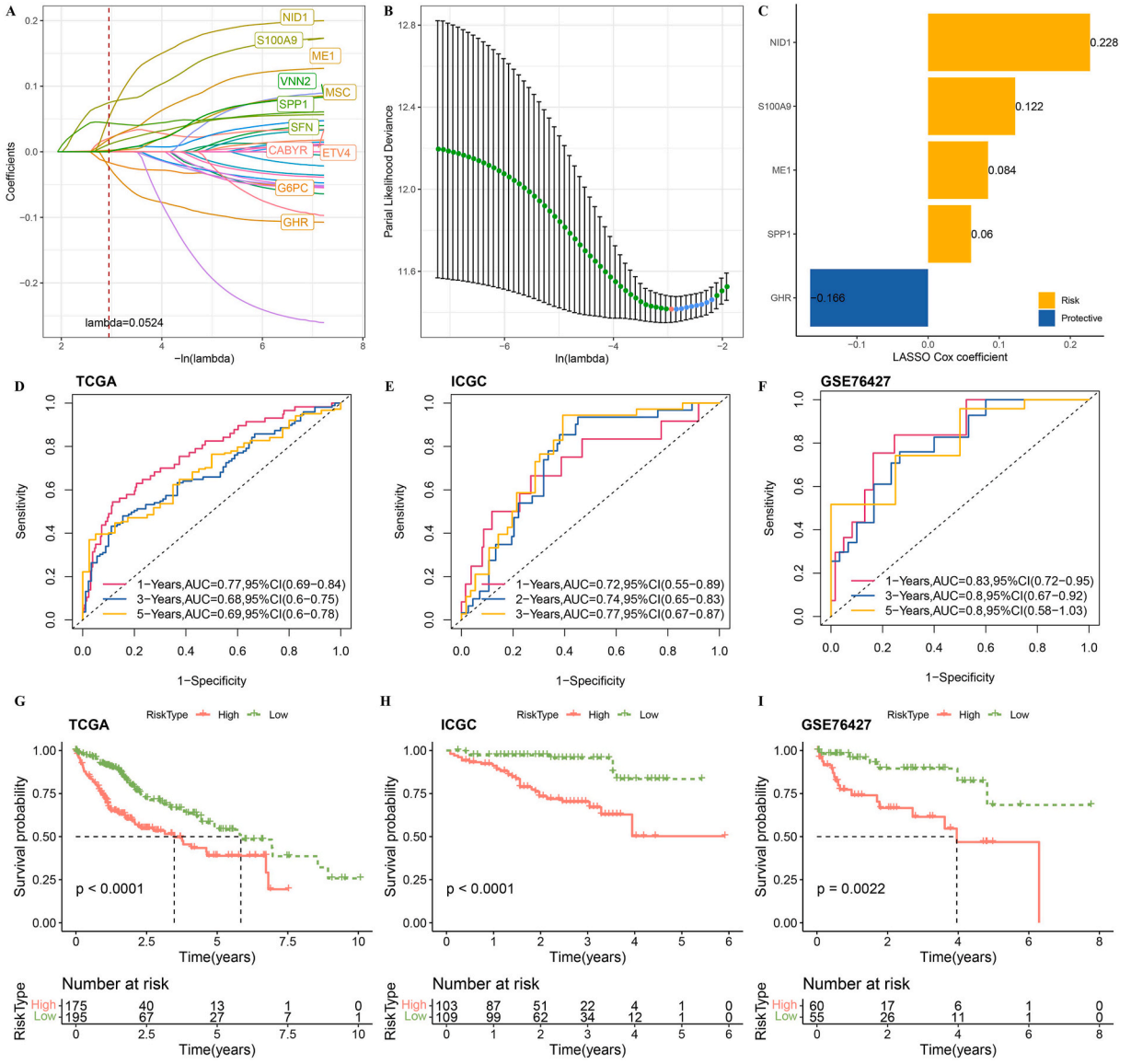

Fig. 6. Construction and validation of the prognostic signature
A, Trajectories of each independent variables with lambda. B, The confidence intervals under each lambda. C, Identification of PCD-related genes as prognostically relevant genes in LIHC. D-F, ROC curves of the calculated risk score in the training set TCGA-LIHC and the validation sets ICGC-LIRI-JP and GSE76427. G-I, Survival of patients based on the risk score in the training set TCGA-LIHC and the validation sets ICGC-LIRI-JP and GSE76427.

considered as prognostic genes correlated with PCD using the stepwise multivariate regression analysis (Fig. 6C).

The risk score was calculated as the following formula:

$$\text{Risk Score} = 0.228 \times \text{NID1} + 0.06 \times \text{SPP1} + 0.122 \times \text{S100A9} + 0.084 \times \text{ME1} + -0.166 \times \text{GHR}$$

The zscore was used to standardize the risk score calculated for both the training set (TCGA-LIHC) and the validation sets (ICGC-LIRI-JP and GSE76427). Then the "timeROC" package was applied for the ROC analysis, and a high predictive performance of the PCD-related prognostic model was observed (Fig. 6D–F). Further, the survival analysis has revealed a lower overall survival chances among high-risk group of patients (Fig. 6G–I) in both the two datasets.

3.7. Correlation between the clinicopathologic characteristics and the risk score

From Fig. 7A and B, remarkable differences in the risk score between patients at different T stages, Stages and Grades could be observed, with higher risk score correlating with higher clinical grades. Also, there were also significant distribution differences in T

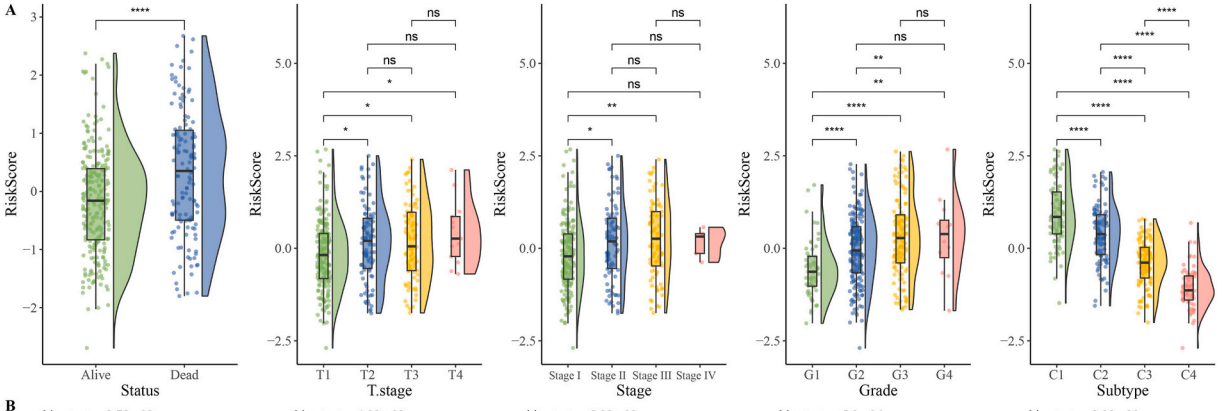

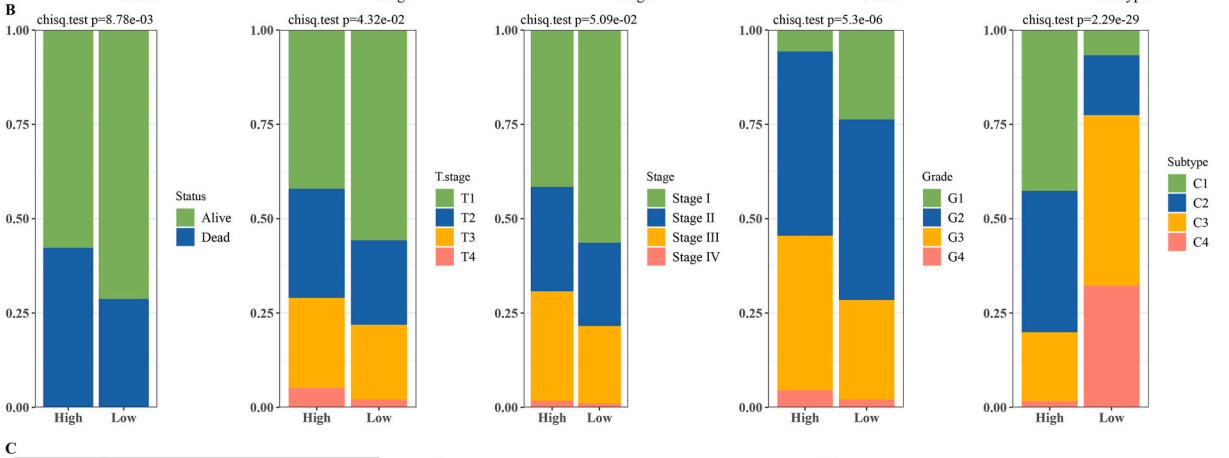

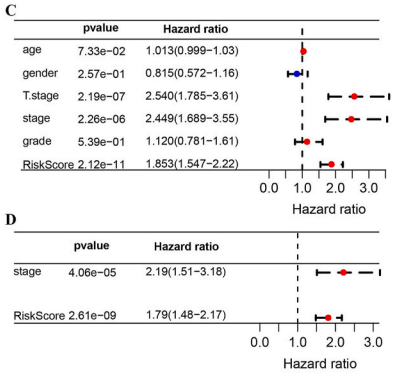

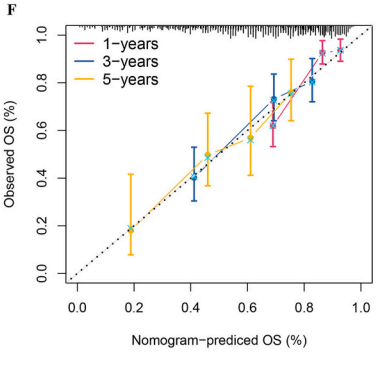

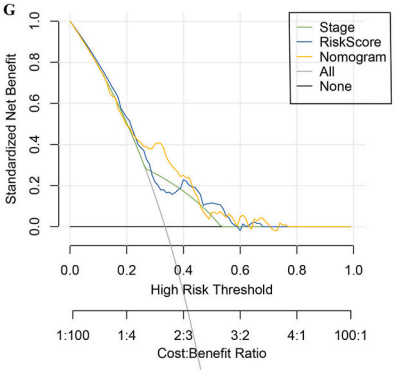

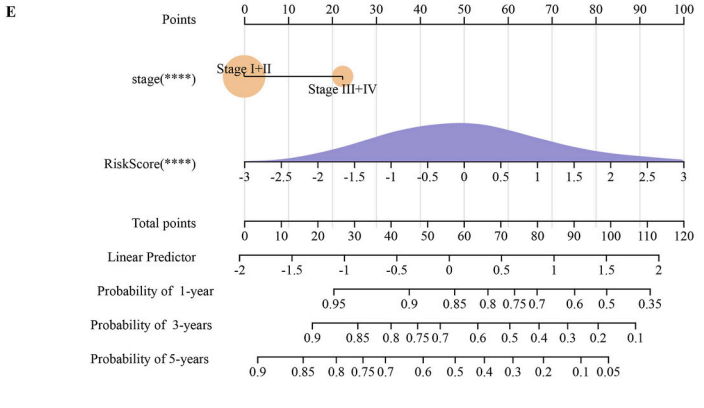

(caption on next page)

Fig. 7. Relationship between risk score and the clinicopathologic features.
A-B, Relationship between the molecular subtypes and clinicopathologic features in TCGA-LIHC cohort. C-D, Results of univariate Cox regression analysis and multivariate Cox regression analysis. E, Constructed nomogram incorporating the RiskScore and other clinicopathologic features. F, Calibration curves evaluating the accuracy on the prediction of survival probability. G, Decision curve drawn to evaluate the reliability of the model. ns represents$P > 0.05$. *$P < 0.05$; **$P < 0.01$; ****$P < 0.0001$.

stages, Stages and Grade in high and low risk score groups.

Correlation analysis between the molecular subtypes and the high/low risk score demonstrated that most patients of high risk group were categorized as C1 and C2, whereas most patients of the low risk group were classified to C3 and C4. Comparison on the risk score differences in these 4 molecular subtypes showed the highest risk score in C1 subtype, followed by C2 subtype, while C4 subtype had the lowest risk score.

Whether the risk score was a clinical prognostic factor independent of other factors (Stage, Grade, age, and gender) in the TCGA-LIHC cohort was analyzed using univariate and multivariate Cox regression analyses (Fig. 7C and D). The univariate analysis showed the significant correlation between overall survival and the risk score. Further, multivariate analysis also verified that the risk score was an independent factor for LIHC prognosis. To further improve the risk assessment and survival evaluation for patients suffering from LIHC, we built a nomogram incorporating the risk score and other clinicopathologic features (Fig. 7E). The results demonstrated that the risk score had the strongest influence on evaluating the survival chances for LIHC patients. Moreover, the calibration curves for 1 year, 3 years and 5 years were close to the standard curves, showing a strong prediction performance of the nomogram. The decision curve (DCA) also showed greater benefit of both the nomogram and risk score and supported their strong capability to predict the survival for LIHC patients.

3.8. Correlation between immune microenvironment and risk score

In this phase, TIMER, EPIC, and MCP-counter were applied to estimate the degree of immune cells infiltration in high/low risk group of the TCGA cohort. In Fig. 8A–C, immune cells and stromal cells were enriched in high-risk group. Also, CIBERSORT results presented significant differences in the abundance of immune cells in the two risk groups, with the high-risk group showing an evident enrichment of Treg and Macrophages_M0 (Fig. 8D). Relevant results on the expression levels of T cell exhaustion markers in high/low risk group have demonstrated the relatively higher expression of TIM-3, TIGIT, PD-1, PD-L1, and LAG-3 in high risk group (Fig. 8E). Evaluation of potential efficacy of immunotherapy to patients in the two risk groups using TIDE software showed higher TIDE score and T cell exclusion score in the high-risk group (Fig. 8F).

3.9. Analysis on LIHC patients' response to immunotherapy

A total of 25 small molecule drugs were identified to be significantly related to the risk score in TCGA-LIHC dataset (Fig. 9A). Notably, the correlation between 5.Fluorouracil and the risk score was shown in Fig. 9B. Further results have confirmed the higher IC_{50} value of 5.Fluorouracil in low-risk group (Fig. 9C), which indicated that high-risk LIHC patients may have a higher sensitivity to 5. Fluorouracil.

4. Discussion

Prognostic relevance of PCD-correlated genes in LIHC and subtyping of LIHC using PCD-correlated genes have been extensively studied in recent years [29,30]. This study used PCD-related genes to classify 4 molecular subtypes, which were distinct in prognostic features, genomic landscape, immune microenvironment and pathways involved. Five PCD-related gene biomarkers, including 4 "Risk" genes and 1 "Protective" gene, were screened based on the co-DEGs in the 4 molecular subtypes and used for the development and verification of a PCD-related prognostic signature. Further validation testified the robustness of the signature in predicting the therapeutic response and prognosis of LIHC patients and its stable predictive values in external dataset.

Several existing studies have employed PCD-related genes for the subtyping of LIHC. He and colleagues [30] identified 52 differentially expressed PCD-related genes to classify 2 clusters for LICH, with cluster 2 showing a worse prognosis in comparison to cluster 1. Further LASSO analysis determined 10 feature genes and used them to calculate the programmed cell death index (PCDI). LIHC patients can be divided into low-PCDI and high-PCDI groups using the PCDI, with high PCDI-group showing a worse prognosis. Another study of Liu has identified 9 immunogenic cell death (ICD)-related gene biomarkers, and these genes can also predict high and low risks for patients, with high-risk group having a relatively poorer prognosis [31]. A gene model consisting of 5 autophagy-, 3 ferroptosis- and 2 pyroptosis-related DEGs can accurately predict a better survival for low-risk patients [15]. In our current study, 335 prognostic gene biomarkers in TCGA-LIHC cohort were identified and applied for consensus clustering, and 4 molecular subtypes were categorized. The worst prognosis was in subtype 1, which had higher numbers of Segs with LOH and fraction of Segs with LOH, number of segments, homologous recombination defects, fraction altered, aneuploidy score, intratumor heterogeneity. Additionally, subtype C1 also had higher ssGSEA score of metastasis-related pathways and significant enrichment of Tregs and Macrophages_M0 as well as higher expression of PD-1, PD-L1, LAG-3, TIM-3 and TIGIT (which were associated with poor prognosis in LIHC patients) [32–35]. Further results showed that the therapeutic response of subtype C1 was less active, providing novel for the classification of LIHC and potential treatment guidance for the cancer.

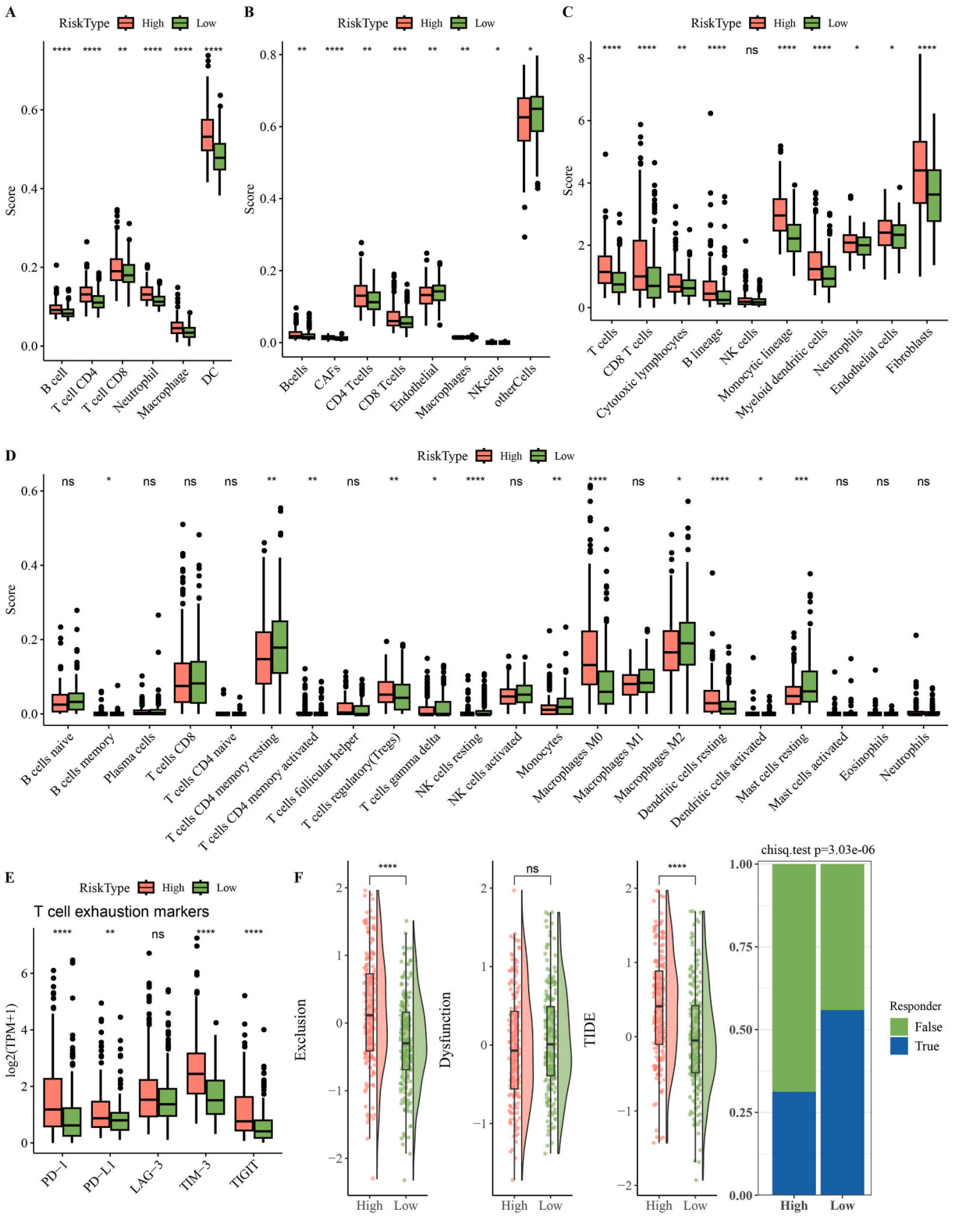

(caption on next page)

Fig. 8. Analysis on the immune microenvironment in high/low risk group of TCGA cohort.
A-D, Immune cells score in high/low risk group of TCGA-LIHC cohort, as determined via TIMER, EPIC, MCP-counter and CIBERSORT. E, Expression levels of T cell exhaustion markers in high/low risk group of TCGA-LIHC cohort. F, Differences on the predicted T cell dysfunction scores, T cell exclusion scores and TIDE score in high/low risk group of TCGA-LIHC cohort. ns represents$P > 0.05$. *$P < 0.05$; **$P < 0.01$; ***$P < 0.001$; ****$P < 0.0001$.

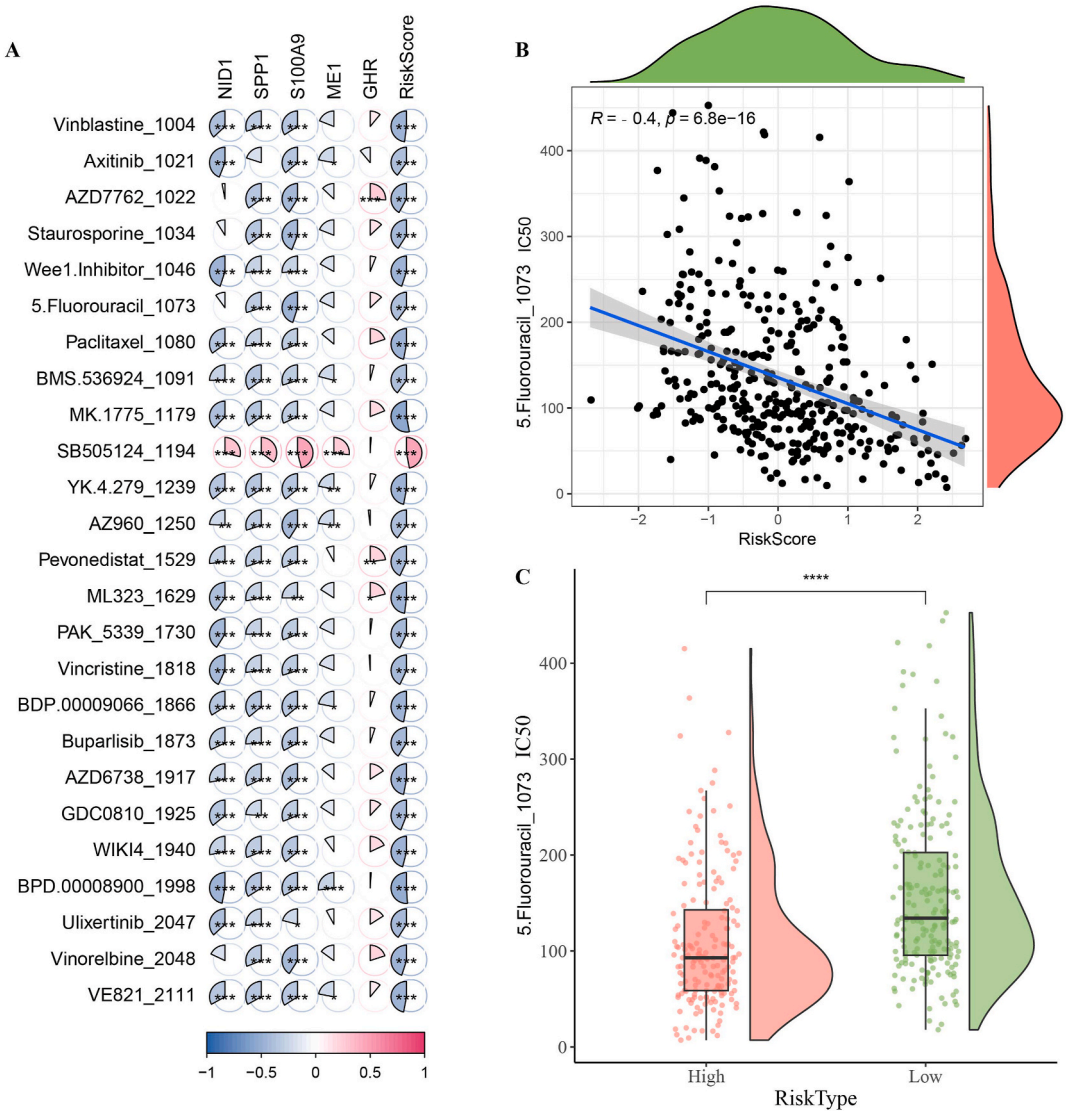

Fig. 9. Analysis on the response of high/low risk group of TCGA cohort to immunotherapy.
A, Correlation between the RiskScore and the small molecule drugs. B, Correlation between the IC_{50} value of 5.Fluorouracil and the RiskScore. C, Boxplots comparing the IC_{50} value of 5.Fluorouracil in high/low risk groups in TCGA cohort. ****$P < 0.0001$.

Five PCD-related prognostic gene biomarkers, including 4 "Risk" genes (NID1, S100A9, ME1 and SPP1) and 1 "Protective" gene (GHR), were identified in our study. NID1 gene is located at 1q42.3, which encodes a member of the nidogen family of basement membrane glycoproteins and is involved in diverse types of cancers including in LIHC [36,37]. S100A9 is a Ca^{2+} binding protein that belongs to the S100 family. S100A9 is also widely reported to be implicated in diverse signaling pathways of tumor cells such as LIHC [38]. ME1 is a multifunctional enzyme associated with lipid metabolism that can induce epithelial-mesenchymal transition in a reactive oxygen species (ROS)-dependent manner, and has been applied for the development of lipid metabolism-based risk score model for LIHC patients [39]. SPP1 is an integrin-binding glycoprotein overexpressed in a variety of tumors, including in HCC [40]. GHR is a prototypical class I cytokine receptor involved in LIHC and is predictive of the prognostic outcomes of LIHC [41,42]. These PCD-related prognostic genes could be used to investigate the molecular mechanisms of LIHC and predict the prognosis and

therapeutic responses for patients with LIHC.

An existing study showed lower imputed sensitive scores of paclitaxel, docetaxel, vinblastine, cediranib, and bortezomib in high PCDI group [10]. Another immune-related gene signature constructed by Shen et al. confirmed a relatively higher sensitivity of high-risk patients to 5-Fluorouracil, VX-11e and sapitnib [43]. Also, molecular subtyping based on a PANoptosis ('P' represents pyroptosis, 'A' represents apoptosis, and 'N' represents necroptosis) can predict the therapeutic response and survival in HCC, with low HPAN-index group showing a significantly higher sensitivity to small molecule inhibitors [7]. Our current study observed a higher IC_{50} value of 5.Fluorouracil in low RiskScore group, which indicated that patients with a high risk score had higher sensitivity to 5. Fluorouracil. Some of the prognostic PCD-related gene biomarkers, for instance, NID1 and S100A9, have been considered as the potential biomarkers for chemoresistance in cancers [40,44]. Thus, it could be speculated that the PCD-correlated gene model developed in the current study may provide novel insight for selecting therapeutic drugs for LIHC patients with different molecular subtypes or risks.

However, there were some limitations of this study. Firstly, the accuracy of the PCD-related gene signature was tested in external datasets from public database, and a clinical validation is required to verify the current conclusions. Secondly, the size of samples was relatively small and cohorts with larger number of samples should be employed. Thirdly, future studies are encouraged to conduct cellular or animal experiments, including using cell lines and tumor xenograft models, to explore the potential mechanisms of these PCD genes during the development of LIHC resistant to 5.Fluorouracil and Cisplatin.

5. Conclusions

To conclude, 4 PCD-based molecular subtypes of LIHC were classified by the current research, providing novel insights for the clinical classification of LIHC patients. Accordingly, a prognostic signature consisting of 5 PCD gene biomarkers was established and validated to be able to evaluate the therapeutic responses and prognosis of LIHC patients. It was hoped that the discoveries in this preliminary study can contribute to the subtyping of LIHC and personalized therapy for patients suffering from LIHC.

Funding

The authors receive no funding to this study.

Data availability statement

The datasets generated and/or analyzed during the current study are available in the [GSE76427] repository, [https://www.ncbi.nlm.nih.gov/geo/query/acc.cgi?acc=GSE76427].

Ethnic statement

Not applicable.

CRediT authorship contribution statement

Lijun Tian: Writing – review & editing, Writing – original draft, Software, Resources, Project administration, Methodology, Data curation, Conceptualization. **Yujie Sang:** Writing – review & editing, Validation, Resources, Methodology, Conceptualization. **Bing Han:** Validation, Supervision, Resources, Project administration, Investigation, Conceptualization. **Yujing Sun:** Visualization, Supervision, Project administration, Conceptualization. **Xueyan Li:** Visualization, Supervision, Resources, Formal analysis. **Yuemin Feng:** Visualization, Resources, Project administration, Methodology, Data curation, Conceptualization. **Chengyong Qin:** Writing – original draft, Visualization, Resources, Methodology, Investigation. **Jianni Qi:** Writing – original draft, Visualization, Validation, Methodology, Data curation, Conceptualization.

Declaration of competing interest

The authors declare that they have no known competing financial interests or personal relationships that could have appeared to influence the work reported in this paper.

Acknowledgments

None.

Abbreviations

(LC) Liver cancer
(LIHC) Liver hepatocellular carcinoma
(PCD) Programmed cell death

(DEGs) differentially expressed genes
(TME) tumor microenvironment
(HCCDB) Hepatocellular Carcinoma Database
(CDF) cumulative distribution function
(FDR) false discovery rate
(ROC) receiver operating characteristic
(GSEA) Gene set enrichment analysis
(KEGG) Kyoto Encyclopedia of Genes and Genomes
(DCA) decision curve
(PCDI) programmed cell death index
(ICD) immunogenic cell death
(ROS) reactive oxygen species

References

[1] G. Zhou, P.P.C. Boor, M.J. Bruno, D. Sprengers, J. Kwekkeboom, Immune suppressive checkpoint interactions in the tumour microenvironment of primary liver cancers, Br. J. Cancer 126 (1) (2022) 10–23.
[2] S. Chidambaranathan-Reghupaty, P.B. Fisher, D. Sarkar, Hepatocellular carcinoma (HCC): epidemiology, etiology and molecular classification, Adv. Cancer Res. 149 (2021) 1–61.
[3] Y.-C. Chen, H.-H. Chen, P.-M. Chen, Catalase expression is an independent prognostic marker in liver hepatocellular carcinoma, Oncologie 26 (1) (2024) 79–90.
[4] Z.J. Brown, D.I. Tsilimigras, S.M. Ruff, A. Mohseni, I.R. Kamel, J.M. Cloyd, et al., Management of hepatocellular carcinoma: a review, JAMA surgery 158 (4) (2023) 410–420.
[5] X. Yang, C. Yang, S. Zhang, H. Geng, A.X. Zhu, R. Bernards, et al., Precision treatment in advanced hepatocellular carcinoma, Cancer Cell 42 (2) (2024) 180–197.
[6] C. Yang, H. Zhang, L. Zhang, A.X. Zhu, R. Bernards, W. Qin, et al., Evolving therapeutic landscape of advanced hepatocellular carcinoma, Nat. Rev. Gastroenterol. Hepatol. 20 (4) (2023) 203–222.
[7] F. Song, C.G. Wang, J.Z. Mao, T.L. Wang, X.L. Liang, C.W. Hu, et al., PANoptosis-based molecular subtyping and HPAN-index predicts therapeutic response and survival in hepatocellular carcinoma, Front. Immunol. 14 (2023) 1197152.
[8] J.M. Schattenberg, M. Schuchmann, P.R. Galle, Cell death and hepatocarcinogenesis: dysregulation of apoptosis signaling pathways, J. Gastroenterol. Hepatol. 26 (Suppl 1) (2011) 213–219.
[9] R.F. Schwabe, T. Luedde, Apoptosis and necroptosis in the liver: a matter of life and death, Nat. Rev. Gastroenterol. Hepatol. 15 (12) (2018) 738–752.
[10] Y. Shi, Y. Feng, P. Qiu, K. Zhao, X. Li, Z. Deng, et al., Identifying the programmed cell death index of hepatocellular carcinoma for prognosis and therapy response improvement by machine learning: a bioinformatics analysis and experimental validation, Front. Immunol. 14 (2023) 1298290.
[11] A.P. Mishra, B. Salehi, M. Sharifi-Rad, R. Pezzani, F. Kobarfard, J. Sharifi-Rad, et al., Programmed cell death, from a cancer perspective: an overview, Mol. Diagn. Ther. 22 (3) (2018) 281–295.
[12] F. Peng, M. Liao, R. Qin, S. Zhu, C. Peng, L. Fu, et al., Regulated cell death (RCD) in cancer: key pathways and targeted therapies, Signal Transduct. Targeted Ther. 7 (1) (2022) 286.
[13] S. Bedoui, M.J. Herold, A. Strasser, Emerging connectivity of programmed cell death pathways and its physiological implications, Nat. Rev. Mol. Cell Biol. 21 (11) (2020) 678–695.
[14] Y. Chen, L. Tang, W. Huang, F.H. Abisola, Y. Zhang, G. Zhang, et al., Identification of a prognostic cuproptosis-related signature in hepatocellular carcinoma, Biol. Direct 18 (1) (2023) 4.
[15] Z. Zhang, X. Zeng, Y. Wu, Y. Liu, X. Zhang, Z. Song, Cuproptosis-related risk score predicts prognosis and characterizes the tumor microenvironment in hepatocellular carcinoma, Front. Immunol. 13 (2022) 925618.
[16] M. Deng, S. Sun, R. Zhao, R. Guan, Z. Zhang, S. Li, et al., The pyroptosis-related gene signature predicts prognosis and indicates immune activity in hepatocellular carcinoma, Mol. Med. (Camb.) 28 (1) (2022) 16.
[17] Y. Zou, J. Xie, S. Zheng, W. Liu, Y. Tang, W. Tian, et al., Leveraging diverse cell-death patterns to predict the prognosis and drug sensitivity of triple-negative breast cancer patients after surgery, Int. J. Surg. 107 (2022) 106936.
[18] M.D. Wilkerson, D.N. Hayes, ConsensusClusterPlus: a class discovery tool with confidence assessments and item tracking, Bioinformatics 26 (12) (2010) 1572–1573.
[19] M.E. Ritchie, B. Phipson, D. Wu, Y. Hu, C.W. Law, W. Shi, et al., Limma powers differential expression analyses for RNA-sequencing and microarray studies, Nucleic Acids Res. 43 (7) (2015) e47.
[20] J. Friedman, T. Hastie, R. Tibshirani, Regularization paths for generalized linear models via coordinate descent, J. Stat. Software 33 (1) (2010) 1–22.
[21] T. Hastie, J. Qian, K. Tay, An Introduction to Glmnet, CRAN R Repositary, 2021.
[22] X. Lin, C. Tian, F. Pan, R. Wang, A novel immune-associated prognostic signature based on the immune cell infiltration analysis for hepatocellular carcinoma, Oncologie 26 (1) (2024) 91–103.
[23] P. Blanche, J.F. Dartigues, H. Jacqmin-Gadda, Estimating and comparing time-dependent areas under receiver operating characteristic curves for censored event times with competing risks, Stat. Med. 32 (30) (2013) 5381–5397.
[24] P. Blanche, TimeROC: time-dependent ROC curve and AUC for censored survival data, R package version 2 (2015).
[25] G. Yu, L.G. Wang, Y. Han, Q.Y. He, clusterProfiler: an R package for comparing biological themes among gene clusters, OMICS A J. Integr. Biol. 16 (5) (2012) 284–287.
[26] B. Chen, M.S. Khodadoust, C.L. Liu, A.M. Newman, A.A. Alizadeh, Profiling tumor infiltrating immune cells with CIBERSORT, Methods Mol. Biol. 1711 (2018) 243–259.
[27] D. Maeser, R.F. Gruener, R.S. Huang, oncoPredict: an R package for predicting in vivo or cancer patient drug response and biomarkers from cell line screening data, Briefings Bioinf. 22 (6) (2021).
[28] V. Thorsson, D.L. Gibbs, S.D. Brown, D. Wolf, D.S. Bortone, T.H. Ou Yang, et al., The immune landscape of cancer, Immunity 48 (4) (2018), 812-30.e14.
[29] H. Zhang, P. Dong, H. Fan, H. Liang, K. Zhang, Y. Zhao, et al., Gene body hypomethylation of pyroptosis-related genes NLRP7, NLRP2, and NLRP3 facilitate non-invasive surveillance of hepatocellular carcinoma, Funct. Integr. Genom. 23 (2) (2023) 198.
[30] Z. He, J. Zhang, W. Huang, Diagnostic role and immune correlates of programmed cell death-related genes in hepatocellular carcinoma, Sci. Rep. 13 (1) (2023) 20509.
[31] T. Liu, X. Chen, B. Peng, C. Liang, H. Zhang, S. Wang, A novel prognostic model based on immunogenic cell death-related genes for improved risk stratification in hepatocellular carcinoma patients, J. Cancer Res. Clin. Oncol. 149 (12) (2023) 10255–10267.

[32] H.I. Jung, D. Jeong, S. Ji, T.S. Ahn, S.H. Bae, S. Chin, et al., Overexpression of PD-L1 and PD-L2 is associated with poor prognosis in patients with hepatocellular carcinoma, Cancer research and treatment 49 (1) (2017) 246–254.
[33] M. Guo, F. Qi, Q. Rao, J. Sun, X. Du, Z. Qi, et al., Serum LAG-3 predicts outcome and treatment response in hepatocellular carcinoma patients with transarterial chemoembolization, Front. Immunol. 12 (2021) 754961.
[34] F. Liu, Y. Liu, Z. Chen, Tim-3 expression and its role in hepatocellular carcinoma, J. Hematol. Oncol. 11 (1) (2018) 126.
[35] Q. Liang, Y. Ye, E. Li, J. Fan, J. Gong, J. Ying, et al., A circadian clock gene-related signature for predicting prognosis and its association with sorafenib response in hepatocellular carcinoma, Transl. Cancer Res. 12 (10) (2023) 2493–2507.
[36] L.E.B. de Mello, T.N.R. Carneiro, A.N. Araujo, C.X. Alves, P.A.F. Galante, V.C. Buzatto, et al., Identification of NID1 as a novel candidate susceptibility gene for familial non-medullary thyroid carcinoma using whole-exome sequencing, Endocrine connections 11 (1) (2022).
[37] X. Mao, S.K. Tey, C.L.S. Yeung, E.M.L. Kwong, Y.M.E. Fung, C.Y.S. Chung, et al., Nidogen 1-enriched extracellular vesicles facilitate extrahepatic metastasis of liver cancer by activating pulmonary fibroblasts to secrete tumor necrosis factor receptor 1, Adv. Sci. 7 (21) (2020) 2002157.
[38] C. Zhong, Y. Niu, W. Liu, Y. Yuan, K. Li, Y. Shi, et al., S100A9 derived from chemoembolization-induced hypoxia governs mitochondrial function in hepatocellular carcinoma progression, Adv. Sci. 9 (30) (2022) e2202206.
[39] W. Wang, C. Zhang, Q. Yu, X. Zheng, C. Yin, X. Yan, et al., Development of a novel lipid metabolism-based risk score model in hepatocellular carcinoma patients, BMC Gastroenterol. 21 (1) (2021) 68.
[40] J.W. Eun, J.H. Yoon, H.R. Ahn, S. Kim, Y.B. Kim, S.B. Lim, et al., Cancer-associated fibroblast-derived secreted phosphoprotein 1 contributes to resistance of hepatocellular carcinoma to sorafenib and lenvatinib, Cancer Commun. 43 (4) (2023) 455–479.
[41] A.O. Kaseb, A. Haque, D. Vishwamitra, M.M. Hassan, L. Xiao, B. George, et al., Blockade of growth hormone receptor signaling by using pegvisomant: a functional therapeutic strategy in hepatocellular carcinoma, Front. Oncol. 12 (2022) 986305.
[42] S. He, J. Qiao, L. Wang, L. Yu, A novel immune-related gene signature predicts the prognosis of hepatocellular carcinoma, Front. Oncol. 12 (2022) 955192.
[43] B. Shen, G. Zhang, Y. Liu, J. Wang, J. Jiang, Identification and analysis of immune-related gene signature in hepatocellular carcinoma, Genes 13 (10) (2022).
[44] X. Hua, H. Zhang, J. Jia, S. Chen, Y. Sun, X. Zhu, Roles of S100 family members in drug resistance in tumors: status and prospects, Biomedicine & pharmacotherapy = Biomedecine & pharmacotherapie 127 (2020) 110156.